Coherence-Protected Quantum Gate by Continuous Dynamical Decoupling in Diamond

Xiangkun Xu, Zixiang Wang, Changkui Duan, Pu Huang, Pengfei Wang, Ya Wang, Nanyang Xu, Xi Kong, Fazhan Shi, Xing Rong, and Jiangfeng Du*

Hefei National Laboratory for Physics Sciences at Microscale and Department of Modern Physics, University of Science and Technology of China, Hefei 230026, China

(Received 2 May 2012; published 16 August 2012)

In order to achieve reliable quantum-information processing results, we need to protect quantum gates along with the qubits from decoherence. Here we demonstrate experimentally on a nitrogen-vacancy system that by using a continuous-wave dynamical decoupling method, we might not only prolong the coherence time by about 20 times but also protect the quantum gates for the duration of the controlling time. This protocol shares the merits of retaining the superiority of prolonging the coherence time and at the same time easily combining with quantum logic tasks. This method can be useful in tasks where the duration of quantum controlling exceeds far beyond the dephasing time.

DOI: 10.1103/PhysRevLett.109.070502 PACS numbers: 03.67.Pp, 03.65.Yz, 33.35.+r, 76.30.Mi

Decoherence of the quantum system is one of the main obstacles to the realization of quantum-information processing, quantum simulation, and quantum sensing [1,2]. Quantum gates, as primary elements for large-scale universal quantum-information processing, are unavoidably affected by decoherence and have to be implemented within the coherence time. Therefore, a qubit needs to be protected not only when it is idle but also during the process of quantum gate operations. Among the various approaches to quantum coherence protection, dynamical decoupling (DD) [3] is a particularly promising strategy due to its integratability with quantum gates by elaborate designs.

Protecting quantum logic tasks with pulsed DD has been proposed [4–8] and experimentally demonstrated in a few quantum systems for extending the coherence time of individual qubit [9–13] and two-qubit entanglement [14]. Despite the great success of pulsed DD in protecting the coherence, it becomes complicated when combined with quantum gates by considering the commutation between the decoupling pulses and the control pulses, which is by no means a trivial task. This can be seen from the recent demonstration on the single nitrogen-vacancy (NV) center by adapting the time intervals between the DD pulses [15].

In order to retain the flexibility of carrying out quantum logic tasks while the qubits are protected, we need to develop continuous-wave dynamical decoupling (CWDD) approaches [16–20]. The application of CWDD to quantum gate protection has been implemented only very recently to trapped ions [21]. In this Letter, we present the combination of CWDD and quantum gates in a solid-state NV center system in diamond. By applying continuous microwave driving fields to the NV system, the decoherence is suppressed and the coherence time is extended by more than an order of magnitude, and by encoding the qubit in a microwave dressed state, the performance of quantum gate has been protected far beyond the quantum system's free-induction decay (FID) time at room temperature. We show that while retaining the superiority of prolonging the coherence time, protected quantum logic tasks can be implemented in an almost trivial manner.

An NV center system is deliberately chosen in this study for its potential in solid-state quantum computing. NV centre spin qubits are promising for quantum-information processing due to their fast resonant spin manipulation [22], long coherence time [23], and easy initialization and readout by laser [24]. However, since the long coherence time of the NV center is not immediately exploitable [23], one has to decouple the NV center from the magnetic interactions with its spin-based environment [10,11]. To fully exploit the merits of NV centers for quantum-information processing, it is essential to decouple the NV centers from the unwanted magnetic interaction with their spin-based environment, while at the same time implementing the desired quantum gate operations.

Here is the theory for the protection of the qubit and the quantum logic for a single NV center using the CWDD method. The electronic spin ground states of an NV center in an external field B_z along the symmetry axis can be described by the following Hamiltonian:

$$H = DS_z^2 + \gamma_e B_z S_z. \tag{1}$$

The zero-field splitting with $D = 2.87$ GHz and the Zeeman term with $\gamma_e = 2.802$ MHz determine the eigenstates $|M_s\rangle$ ($M_s = \pm 1, 0$), shown in Fig. 1(a) by thick lines. The loss of quantum coherence of the NV center in type IIa diamond is mainly caused by the surrounding ^{13}C nuclear spin bath fluctuations [25,26]. This can be described by an effective weak random magnetic field b with time correlation [10]. The linear dependence of the energies $|\pm 1\rangle$ on the magnetic field [Fig. 1(b)] results in a sharp variation of the energy gap $\omega_{0,-1}$ [Fig. 1(c)] between the two states of the qubit ($|0\rangle$ and $|-1\rangle$). This results in strong decoherence due to the random magnetic field b..

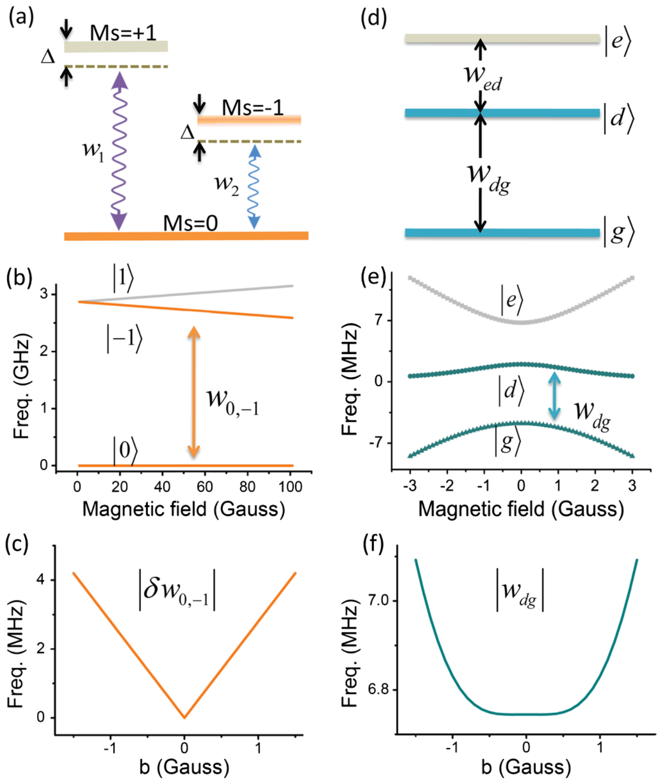

FIG. 1 (color online). (a) The electron spin-triplet states (thick solid lines) of NV center in an external magnetic field B_z along the symmetry axis ([111] direction). The wavy arrow lines indicate two applied continuous microwaves of frequencies ω_1 and ω_2 with the same Rabi frequency Ω. (b) The splitting of the electron spin-triplet states of NV center with the external magnetic field B_z, with $\omega_{0,-1}$ the energy gap between states $|-1\rangle$ and $|0\rangle$ representing the qubit. (c) The dependence of $|\delta\omega_{0,-1}|$, i.e., the drift of $\omega_{0,-1}$ on the fluctuation field b. (d) The dressed states of the driven NV center system of (a), with ω_{dg} and ω_{ed} showing the corresponding energy gaps. (e) The dependence of the energies of dressed states on the field b. (f) The sensitivity of the ω_{dg} to the fluctuation field b, parameters used: detuning $\Delta = 2$ MHz and Rabi frequency $\Omega = 4\Delta$ for both microwaves.

An equally weighted superposition of $|\pm 1\rangle$ can result in states with eigenvalues insensitive to the random field b. This can be realized by applying two off-resonant continuous microwave driving fields to $|0\rangle \rightarrow |\pm 1\rangle$ at the same time, as shown in Fig. 1(a) by ω_1 and ω_2. The Hamiltonian of the NV center driven by two microwaves of the same off-resonance Δ and Rabi frequency Ω can be written in the interaction picture as follows:

$$H_{\mathrm{NV}} = \sum_{\iota=\pm 1} [(\Delta + \gamma_e b \iota)|\iota\rangle\langle\iota| + \frac{\Omega}{2}(|0\rangle\langle\iota| + |\iota\rangle\langle 0|)]. \quad (2)$$

The diagonalization of H_{NV} results in three dressed states, $|e\rangle$, $|d\rangle$ and $|g\rangle$ in the driven space, as depicted in Fig. 1(d). The two lower levels $|g\rangle$ and $|d\rangle$ of the gap w_{dg} are used as a qubit. Owing to the symmetry of H_{NV} and nonzero Ω, the energies of all the three states are only functions of b^2 [shown in Fig. 1(e)], which are insensitive to b, in contrast to the linear dependence of $|\delta\omega_{0,-1}|$ on $|b|$ shown in Fig. 1(c). Hence, the dephasing between $|d\rangle$ and $|g\rangle$ will be strongly suppressed when the microwave Rabi frequency Ω is much larger than the weak effective random field. With the appropriate ratio of $\Omega/\Delta(=4)$ shown in Fig. 1(f), even the b^2 term in w_{dg} is eliminated so that the lowest order is $\sim b^4$, and a much greater coherence time can be achieved in the protected subspace spanned by $|d\rangle$ and $|g\rangle$ [16]. The gradual transfer from $|0\rangle$ to $|g\rangle$ when the microwave Rabi frequency Ω gradually increases allows adiabatical preparation and readout, and the manipulation of the dressed state can be realized by an RF pulse.

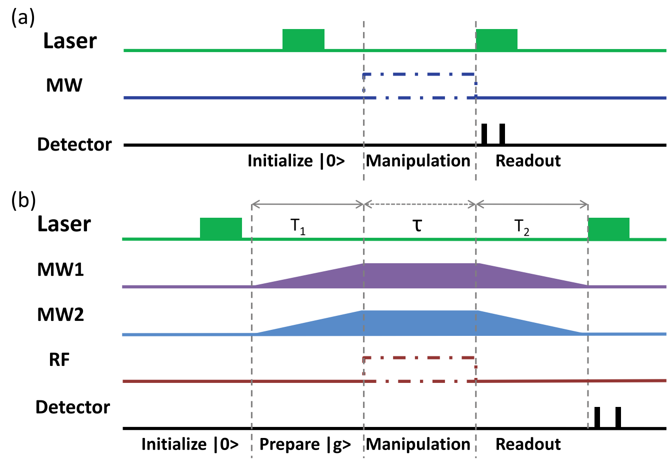

FIG. 2 (color online). Diagram of the experimental pulse sequences used in the experiment. (a) Pulse sequences without CWDD. The electron spin state of the NV center is initialized to $|M_s = 0\rangle$ by the 532 nm laser pulse, manipulated by microwave pulses, and readout through the fluorescence. (b) Pulse sequences with CWDD. The 532 nm laser initializes the electron spin state of the NV center to $|M_s = 0\rangle$. Then the two microwave fields (MW1, MW2) are ramped linearly to time T_1, and the ground state $|g\rangle$ in the driven space is adiabatically prepared. Next, the driving amplitudes are kept constant, during which an additional radio frequency (RF) is applied to realize state manipulation. Finally, the adiabatical process transfers the microwave dressed state in the protected subspace to the bare electronic spin states of the NV center and readout by the fluorescence.

The whole experimental scheme for characterizing the NV center and quantum logic operations for the two cases without and with CWDD are given in Figs. 2(a) and 2(b), respectively. For the undriven case [Fig. 2(a)], the laser pulses are used for initial state preparation and final state readout, and the microwave pulses are used to manipulate the qubit. For the driven case [Fig. 2(b)], after the initialization of $|0\rangle$, two driven microwaves (MW1, MW2) are up-ramped linearly to prepare $|g\rangle$ adiabatically, the RF is used for the qubit manipulation encoded in the driven system with the continuous microwave protection, and finally the down-ramped microwaves map the encoded state $|g\rangle$ ($|d\rangle$) to $|0\rangle$ ($|-1\rangle$) for laser readout.

In this experiment, the sample used is type IIa diamond (with nitrogen density <5 ppb). A 12 Gauss magnetic field generated using three pairs of Helmholtz coils is used to remove the degeneracy of $M_s = \pm 1$ states. The magnetic field is aligned with the NV symmetry axis. Two protecting microwave fields are generated using the sidebands of a local oscillator mixed with an integrated frequency produced by a direct digital synthesizer . The detuning Δ is controlled by an local oscillator . The phase and amplitude of the microwaves (MW1, MW2) used in Fig. 2(b) can be controlled by the direct digital synthesizer. Then, through a linear amplifier (16 W), the microwaves are radiated to the NV center via a 20 μm copper wire with a 50 ohm resist terminator. The controlled RF is provided with a 10 MHz arbitrary waveform generator (AWG) and directly coupled to the copper line. All input signals are synchronized by a pulse generator. The length of the initialization laser pulse is 3 μs and the waiting time following the laser is 5 μs. Photoluminescence is measured during an integration time of 0.35 μs. To suppress the photon statistic error, each measurement is typically repeated more than 10^6 times.

The optical detected magnetic resonance spectrum for $|0\rangle \rightarrow |1\rangle$ transition in the undriven NV system is plotted in Fig. 3(a). The three equally spaced dips determine the three frequencies of ~2.2 MHz separations and show clearly the hyperfine splitting due to the $I = 1$ nuclear spin of ^{14}N. The FID signal for the undriven NV system oscillates and dephases on a fast time scale, as shown in Fig. 3(b). The oscillation of FID is caused by the beats originated from three transitions of different frequencies as a result of hyperfine splitting related to the ^{14}N nuclear spin. The damping of the oscillation of FID signal is well fitted with a Gaussian envelope function $\exp[-(t/T_2^*)^2]$ [10], giving a dephasing time of $T_2^* = 0.93$ μs, which is mainly caused by the nuclear spin bath fluctuation of surrounding ^{13}C. By following Ref. [20], we estimate the strength of the bath field as $b = 1/(2\pi T_2^*) = 0.17$ MHz.

To implement coherence-protected quantum gates, suitable experimental parameters for the detuned driving microwave fields, such as $w_{1,2} = w_{0,\pm1} - \Delta$, their Rabi frequencies, and forward and reversed ramp time, need to be determined, and the corresponding resonant RF w_{dg} needs to be experimentally measured. In the following, we shall only work with the $M_I = 0$ subspace. First, $w_{0,1}$ and $w_{0,-1}$ are accurately determined to an uncertainty of less than 20 KHz. Then, we choose $\Delta = 0.4$ MHz, which is large enough compared to the uncertainty of $w_{0,\pm1}$, yet small enough compared to the hyperfine splitting between $M_I = 0$ and $M_I = \pm 1$. The theoretically optimum condition $\Omega = 4\Delta$ constrains $\Omega \approx 1.6$ MHz. This should be sufficiently large to suppress the relatively weak and slow bath field of ~0.17 MHz in magnitude. Next, a suitable forward and reversed ramp time $T_1 = T_2 = 50$ μs is chosen to satisfy the adiabatic condition. Finally, we determine w_{dg} by sweeping the RF using an RF pulse of a duration of 20 μs. The result is shown in Fig. 3(c). The FID signal for the CWDD-protected subspace $\{|d\rangle, |g\rangle\}$ obtained by applying a detuned RF pulse is shown in Fig. 3(d), where the oscillation reflects the detuning f of the RF. Fitting with $\exp[-(t/T_{2,\mathrm{CWDD}}^*)^2]\cos(2\pi f t + \varphi)$ results in $T_{2,\mathrm{CWDD}}^* = 18.9$ μs. This shows that the coherence time of the CWDD-protected single spin is prolonged by ~20 times from the coherence time of the bare spin (of 0.93 μs) of the NV center.

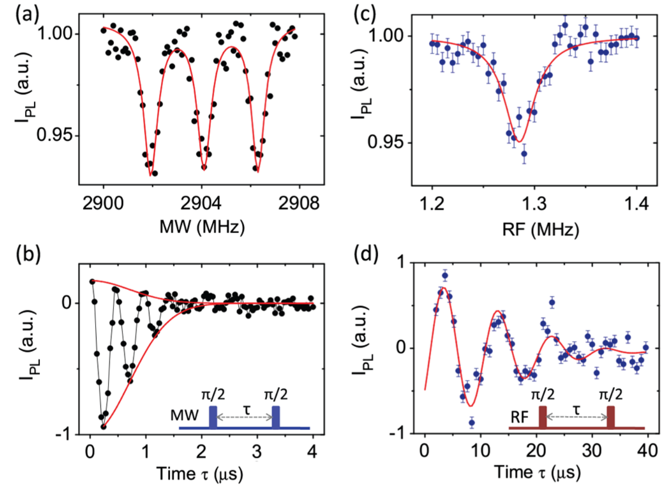

FIG. 3 (color online). (a) The ODMR spectrum for transition between $|0\rangle$ and $|1\rangle$ in NV center (black dots). The smooth curve is the plot to guide the eyes. The three lines due to hyperfine coupling with ^{14}N nuclear spin are resolved. (b) Measured (dots) and fitted FID signals of the NV center. The oscillations and asymmetric envelopes are due to coupling to the ^{14}N nuclear spin. The microwave sequences in the lower right corner is used in the manipulation part in Fig. 2(a). (c) The ODMR spectrum for continuous microwave-driven NV center system. The dip in the figure corresponds to the transition between state $|d\rangle$ and $|g\rangle$. Error bars are standard deviations. (d) Experimental FID signals in the NV center driven system. The RF sequence in the lower right corner is used in the manipulation part in Fig. 2(b) to obtain the signals.

The manipulations of the unprotected qubit using microwave pulses [scheme in Fig. 2(a)] and the protected qubit using RF pulses [scheme in Fig. 2(b)] are carried out to show the performance of the CWDD approach.

Figure 4(a) plots the Rabi oscillation in the $M_s = 0, -1$ bases without the driven and $|d\rangle$, $|g\rangle$ bases with CWDD. It clearly shows that the oscillation in the $|d\rangle$, $|g\rangle$ is well preserved almost without decay even after 25 μs, while that in the $M_s = 0, -1$ bases suffers considerable decay even in a few μs. Because of the complexity of measuring the fidelity of the quantum gate in the protected space, the performance of the CWDD-protected quantum gate is evaluated using the coherence of the state after successive NOT gate operations. The performance of the NOT gate is shown in Fig. 4(b) by plotting the indicator F defined to be

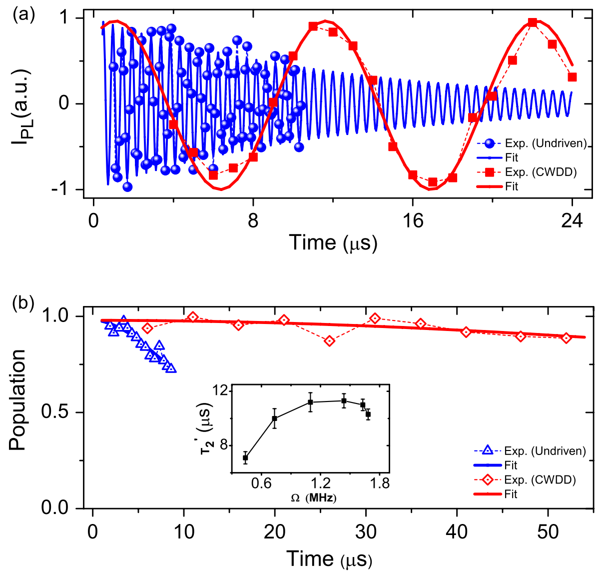

FIG. 4 (color online). (a) Measured decay of Rabi oscillation both in the undriven space (spheres) and in the subspace protected by CWDD (squares); the curve is only for guiding the eyes. (b) The population of the designated state as a result of the successive NOT gate operation in undriven space with microwave π pulse (triangles), or in a CWDD-protected space with RF π pulse (diamonds). The curve is fitted to Gauss lineshape decays. The subset is the measured decay time T_2' as a function of the microwave field amplitude Ω.

$|\langle\psi|d\rangle|^2$ for odd numbers of NOT gates and $\langle\psi|g\rangle|^2$ for even numbers of NOT gates. Compared to the decay time of 11 μs in the undriven case, for the CWDD-driven case, the coherence is maintained far beyond 50 μs, clearly demonstrating the performance of the quantum gate protected with CWDD.

From the point of view of suppressing noise, just like the noise of the undriven NV system being suppressed by the microwave pulse of the successive NOT gates, the noise felt by the states in the driven subspace $\{|d\rangle, |g\rangle\}$ is also suppressed by the RF pulse of the NOT gates. This is shown clearly in Fig. 4, where the decay time of the protected gates (far beyond 50 μs) is much longer than the FID time of 18.9 μs for the protected subspace.

To further understand the decay of the coherence in Fig. 4, we plot as an inset of Fig. 4(b) the measured T_2' of the undriven states of the NV center as a function of the identical amplitude for the two driven microwave fields of frequencies $w_{0,\pm1}$. It clearly shows that T_2' first increases and then decreases fast with the increasing microwave strength. Suppression of the nuclear bath by the driven microwave field and the fluctuation of the driven microwave field lead to the increase and decrease of T_2', respectively. The latter is similar to previous experiments [27]. When the microwave field amplitude is small, the fluctuation amplitude is also small, and the main contribution to dephase is from the restrained bath fluctuation, which leads to an increase of T_2'. As the microwave field amplitude increases further, its fluctuation becomes larger, and eventually its effect exceeds that of the bath fluctuation, which leads to a sharp decrease of T_2'. Hence, if the microwave field strength were more stable or its fluctuation were suppressed with second-order RF driving fields, we can expect further increase of the coherence time.

Conclusions and outlook.—We have realized CWDD in a solid-state system, i.e., a single NV center in diamond. The coherence time of the NV center is prolonged by about 20 times with CWDD. What is more important, we could combine the CWDD with quantum gate operation. The performance of the quantum gate of a given duration is greatly improved compared to the same quantum manipulation without CWDD. By this, we have paid the price of reducing the gate speed, which could be faster in principle provided the driving MW fields were stronger and more stable. In principle, the CWDD scheme can be generalized to the situation of a magnetic dipole-mediated two-qubit gate between NV centers while maintaining the gate speed. The experimental implementation of CWDD to quantum gate protecting sheds some light here also on more challenging further experiments of applying CWDD to two-qubit gates [20], which is crucial for large-scale quantum-information processing [28] and fault-tolerant quantum computing. The CWDD approach is an alternative method to overcome decoherence, which also has various potential applications including ultrasensitive and nanoscale metrology [16,29]. Although demonstrated on an NV center in diamond here, the method can be applied to other systems also, such as other ion-doped crystals and quantum dots.

This work was supported by the National Natural Science Foundation of China (Grants Nos. 10834005, 91021005, and 11161160553), the Instrument Developing Project of the Chinese Academy of Sciences (Grant No. Y2010025), and the National Fundamental Research Program.

*djf@ustc.edu.cn

[1] M. A. Nielsen and I. L. Chuang, *Quantum Computation and Quantum Information* (Cambridge University Press, Cambridge, England, 2000).
[2] T. D. Ladd, F. Jelezko, R. Laflamme, Y. Nakamura, C. Monroe, and J. L. OBrien, Nature (London) **464**, 45 (2010).
[3] L. Viola, E. Knill, and S. Lloyd, Phys. Rev. Lett. **82**, 2417 (1999).
[4] K. Khodjasteh and D. A. Lidar, Phys. Rev. Lett. **95**, 180501 (2005).
[5] G. S. Uhrig, Phys. Rev. Lett. **98**, 100504 (2007).
[6] W. Yang and R. B. Liu, Phys. Rev. Lett. **101**, 180403 (2008).
[7] B. Lee, W. M. Witzel, and S. D. Sarma, Phys. Rev. Lett. **100**, 160505 (2008).

[8] J. R. West, D. A. Lidar, B. H. Fong, and M. F. Gyure, Phys. Rev. Lett. **105**, 230503 (2010).
[9] J. Du, X. Rong, N. Zhao, Y. Wang, J. Yang, and R. B. Liu, Nature (London) **461**, 1265 (2009).
[10] G. de Lange, Z. H. Wang, D. Rist, V. V. Dobrovitski, and R. Hanson, Science **330**, 60 (2010).
[11] C. A. Ryan, J. S. Hodges, and D. G. Cory, Phys. Rev. Lett. **105**, 200402 (2010).
[12] A. M. Souza, G. A. Alvarez, and D. Suter, Phys. Rev. Lett. **106**, 240501 (2011).
[13] M. J. Biercuk, H. Uys, A. P. VanDevender, N. Shiga, W. M. Itano, and J. J. Bollinger, Nature (London) **458**, 996 (2009).
[14] Y. Wang, X. Rong, P. Feng, W. Xu, B. Chong, J. H. Su, J. Gong, and J. Du, Phys. Rev. Lett. **106**, 040501 (2011).
[15] T. van der Sar, Z. H. Wang, M. S. Blok, H. Bernien, T. H. Taminiau, D. M. Toyli, D. A. Lidar, D. D. Awschalom, R. Hanson, and V. V. Dobrovitski, Nature (London) **484**, 82 (2012).
[16] P. Rabl, P. Cappellaro, M. V. G. Dutt, L. Jiang, J. R. Maze, and M. D. Lukin, Phys. Rev. B **79**, 041302(R) (2009).
[17] J. M. Cai, F. Jelezko, M. B. Plenio, and A. Retzker, arXiv:1111.0930v1.
[18] F. F. Fanchini, J. E. M. Hornos, and R. d. J. Napolitano, Phys. Rev. A **75**, 022329 (2007).
[19] A. Z. Chaudhry and J. B. Gong, Phys. Rev. A **85**, 012315 (2012).
[20] A. Bermudez, F. Jelezko, M. B. Plenio, and A. Retzker, Phys. Rev. Lett. **107**, 150503 (2011).
[21] N. Timoney, I. Baumgart, M. Johanning, A. F. Varon, M. B. Plenio, A. Retzker, and Ch. Wunderlich, Nature (London) **476**, 185 (2011).
[22] G. D. Fuchs, V. V. Dobrovitski, D. M. Toyli, F. J. Heremans, and D. D. Awschalom, Science **326**, 1520 (2009).
[23] G. Balasubramanian, P. Neumann, D. Twitchen *et al.*, Nature Mater. **8**, 383 (2009).
[24] A. Gruber, A. Drabenstedt, C. Tietz, L. Fleury, J. Wrachtrup, and C. von Borczyskowski, Science **276**, 2012 (1997).
[25] P. Huang, X. Kong, N. Zhao, F. Shi, P. Wang, X. Rong, R. B. Liu, and J. Du, Nature Commun. **2**, 570 (2011).
[26] N. Zhao, S. W. Ho, and R. B. Liu, Phys. Rev. B **85**, 115303 (2012).
[27] H. Fedder, F. Dolde, F. Rempp, T. Wolf, P. Hemmer, F. Jelezko, and J. Wrachtrup, Appl. Phys. B **102**, 497 (2011).
[28] N. Y. Yao, L. Jiang, A. V. Gorshkov, P. C. Maurer, G. Giedke, J. I. Cirac, and M. D. Lukin, Nature Commun. **3**, 800 (2012).
[29] J. M. Cai, F. Jelezko, M. B. Plenio, and A. Retzker, arXiv:1112.5502v1.